MINERALOGY ASSOCIATED WITH ACID MINE SEEPAGE AS DETERMINED USING FOURIER TRANSFORM INFRARED SPECTROSCOPY AND RELATIONS TO ACID BASE ACCOUNTING

An Undergraduate Research Scholars Thesis

by

FRANKLIN LINAM

Submitted to the Undergraduate Research Scholars program at
Texas A&M University
in partial fulfillment of the requirements for the designation as an

UNDERGRADUATE RESEARCH SCHOLAR

Approved by Research Advisor: Dr. Youjun Deng

May 2017

Major: Plant & Environmental Soil Science

TABLE OF CONTENTS

ABSTRACT

Mineralogy Associated with Acid Mine Seepage as Determined using Fourier Transform Infrared Spectroscopy and Relations to Acid Base Accounting

Franklin Linam
Department of Soil & Crop Sciences
Texas A&M University

Research Advisor: Dr. Youjun Deng
Department of Soil & Crop Sciences
Texas A&M University

Over 7,000 km of streams in the eastern United States are negatively affected by acid drainage from coal mines (U.S. Environmental Protection Agency, 1994). Pyrite (FeS_2) is known to be the primary cause of acid formation, but analytical measurements to quickly and accurately detect trace pyrite content and predict acid drainage are lacking. This study analyzed sedimentary samples from a reclaimed east Texas lignite mine using Fourier Transform Infrared spectroscopy (FTIR) to detect the pyrite responsible for the environmental degradation of surface waters and the water table due to low (~2.5) pH. Subsequently, acid base accounting (ABA) was used to determine net acid forming potential of the mineralogy and determine FTIR utility.

In conjunction with X-Ray Diffraction data, FTIR spectra and experiments and scanning electron microscopy (SEM) have semi-quantitatively detected the FeS_2 which has and will release the H^+ responsible for the low pH in the surface water bodies. Analytical techniques were used to develop a concept of how acid-formation from mine tailings can be predicted relatively accurately and quickly using FTIR.

ACKNOWLEDGEMENTS

I would like to thank all of the soil mineralogy lab at Texas A&M University. I would particularly like to thank Bidemi Fashina for training and advising me on techniques; Dr. Youjun Deng for allowing me to research in his lab, advising me on research topics and focuses, and editing my writing; and Jason Paul for helping me to organize my time management, and working alongside me on this project the whole way.

Additionally, I would like to thank the Soil & Crop Science Department at Texas A&M University for the financial, academic, and personal support it has shown me during my time here. Specifically, I would like to thank my academic advisor Megan Teel for encouraging and helping me to become involved in undergraduate research and find this opportunity.

TERMINOLOGY

ABA – Acid Base Accounting
AFM – Acid Forming Minerals
AMD – Acid Mine Drainage
FTIR – Fourier Transform Infrared Spectroscopy
SEM – Scanning Electron Microscopy
XRD – X-Ray Diffraction
XRF – X-Ray Fluorescence

CHAPTER I

INTRODUCTION

Acid mine drainage (AMD) is a major environmental and economic problem. Many environments have been degraded by acid mine drainage, and many resources have been spent trying to remedy the effects of acid mine drainage. Mining disrupts the local geology, which can cause acid-forming minerals (AFM) to oxidize and generate H^+ ions, thus lowering the pH. This damages local ecosystems and water sources—not only through lowering pH, but also though mobilizing heavy metals such as arsenic, silver, zinc, and cadmium (U.S. Environmental Protection Agency, 1994). To prevent acid formation problems, the mechanisms of and minerals involved in acid formation must be understood, and methods of quick and accurate analysis need to be developed. The US Forest Service claims that the lack of acid prediction technology is a major problem facing future mining in the western US (U.S. Environmental Protection Agency, 1994), and government agencies alone spent around $200 million annually between 1997 and 2008 on mining site remediation efforts (Mittal, 2011).

In this particular reclaimed mine site in East Texas, acid seepage has caused pH levels to fall to around 2.5 at two ponds. Traditional means of raising the pH is to add NaOH, which can cost hundreds of thousands of dollars annually to maintain neutral pH. Previous work at this site has revealed the presence of pyrite (FeS_2) minerals, which react with oxygen and water to form sulfuric acid (see equation below); however, there are many other minerals which contribute to the geochemistry of the site, as well as variation in size and crystallinity of the pyritic minerals. This project investigated the utility and limits of analytical methods to detect pyrite, which is

assumed to be the main cause of continued acid seepage. Results from this project can be used to devise long-term solutions to this problem, both in this case and in related issues

$$FeS_{2(s)} + 3O_{2(aq)} + 2H_2O \rightarrow Fe^{2+} + 2SO_4^{2-} + 4H^+ \quad (1)$$

elsewhere.

Another facet of this particular issue is the way in which the mine tailings were discarded—namely, in large hills. These hills introduced a spatial component to the weathering and seepage taking place. The catena concept describes spatial soil formation along a hillslope from the top of a peak to the bottom of a valley. Soils develop differently along this catena through variations in water and sediment fluxes and water table effects (Schaetzl & Anderson, 2005). Through manual redeposition of the mine tailings, sediments have been transferred to a new position on the slope. These sediments are now developing according to the catena concept, and these processes are responsible for the acid mine drainage. Data from this project can be used to monitor soil formation and mineral weathering.

FTIR is an analytical technique which uses IR absorption of compounds to identify unknown materials, determine sample consistence, and determine amounts of compounds in mixtures (Thermo Nicolet Corporation, 2001) and has been used with success in mineralogical applications (Xu, et al.). Acid-Base Accounting (ABA) is a method for analyzing materials for their acid potential by measuring and comparing two mineralogical properties: maximum acid potential and neutralization potential of alkaline minerals (Sobek, et. al. 1978). Because of the strongly acidic nature of the sediments in this project, base content was assumed to be neutralized and was not accounted for; solely the acidic minerals were measured.

While FTIR is an entirely conclusive technique in identifying pure or isolated compounds, complex FTIR spectra can be difficult to interpret. Soil and sediment samples are often very heterogeneous, complex mixtures of aluminosilicates, iron and manganese oxides, and

organic polymers and acids. These properties often result in spectral inference from matrix effects (Maciejewska, 2015), which takes the form of overlapping peaks and broadband absorption. Because of this complexity, different techniques must be used to elucidate the compounds present in sediment samples. Spectral subtraction is one such technique.

During subtraction, intensity values from an FTIR spectrum can be subtracted from that of another to yield a difference spectrum which ideally contains all of the peaks present in the original spectrum without the peaks from the subtracted spectrum. This process has been used in many applications, including geologic and soil applications. Aluminosilicates and calcium silicate gel mixtures have been analyzed using FTIR subtraction (Puligilla & Mondal, 2015). Through scanning before and after chemical treatment, overlapping spectra were separated using the differences in solubility of the mixture components. Additionally, quartz content in geologic samples from Poland was determined using FTIR by subtraction of contaminant kaolinite and feldspar FTIR spectra (Maciejewska, 2015). This process eliminated interfering spectra from unwanted minerals and allowed much clearer and more accurate determination of quartz.

A similar concept is proposed in this project. The samples under study are far from geologically pure, and as such, are difficult to analyze with FTIR. Determination of interfering compounds is essential. Most of the samples in this study were dominated by quartz. Quartz is a relatively inert mineral, and is known to not be responsible for, or involved in, acid mine drainage. For this reason, standard quartz FTIR spectra were subtracted from sample FTIR spectra to reveal peaks from other minerals in the FTIR spectra—particularly pyrite. This allowed for more precise mineral identification.

Scanning electron microscopy (SEM) is another technique of frequent use in mineral analysis. SEM has been used in analysis of lignite mine samples to distinguish the different

mineral constituents often present in lignite, such as gypsum, quartz, pyrite, and organics (Predeanu, et al., 2016). SEM was used to positively identify pyrite in the samples and to investigate its structural properties and chemical composition.

The current methods of acid mine drainage mitigation include adding alkali minerals, capping mine tailing heaps, and construction of wetlands for a reducing environment (McClure, 2012). These solutions are expensive and non-specific in regards to mineral type. Identification and monitoring of AFM before and during mining could help developers create proactive plans to prevent acid mine drainage, rather than trying to mitigate the problem after it has developed.

CHAPTER II

MATERIALS AND METHODS

The first step in this analysis was the selection of samples to analyze. Sediment cores from 12 wells with XRF elemental composition measured at 2 foot depth intervals were collected during previous work on this site. After identifying all of the cores, samples were selected based on several factors relating to ABA. A total of 83 samples were chosen for FTIR and XRD analysis based on high iron or sulfur content, anomalous vertical appearance or disappearance of sulfur, and groundwater pH measurements. Additionally, some of the samples were chosen to create a representative view of the total mineral constitution of the sediments. Out of the 83 samples meeting these criteria, three sets totaling 28 representative samples were selected for ABA analysis. The samples represented sediments from various depths from six different cores taken from the study site.

After selection, the sediments were taken out of the -80°C freezer, thawed for 24-48 hours in a refrigerator, and air dried for ~72 hours (*Figures 1*, *2*, and *3*). A vertical cut off of the core was taken to represent all minerals present in the 2 foot interval. These samples were then ground in a mortar and pestle and sifted through a number 140 sieve, which allows passage of particles under 0.105 mm. This finely ground material was then used to record the FTIR-ATR spectra for all samples on a Perkin Elmer Spectrum 100 FTIR Spectrometer with a Universal attenuated total reflectance attachment. Proper cleaning, calibration, and background techniques were practiced during this process in a climate-controlled room. Peaks were identified manually and smoothing was performed if necessary.

Figure 1. Drying samples showing common reduced (L) and oxidized (R) mineral conditions.

Figure 2. Drying samples showing colorations due to lignite (L) and partial oxidation (R).

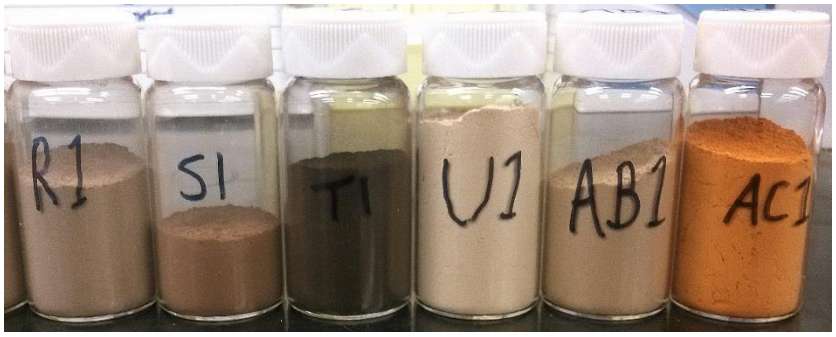

Figure 3. Ground/sieved samples used for FTIR, XRD, and ABA showing mineral variations.

Additionally, the number 140 sieved sediment was used for the XRD analysis. The XRD patterns were recorded by Jason Paul on a Bruker D8 Advance x-ray Diffractometer to generate comparative data for the FTIR results.

ABA procedures were chosen and adapted from O'Shay et al. (1990). In O'Shay et al. (1990), pure pyrite samples were used to develop the procedure, which was successfully employed on potential lignite mine sites in Texas. These methods are an improvement in accuracy over the commonly-employed Sobek methods as the results are not as skewed by the presence of organic matter, reduced iron, and non-sulfate sulfur. Additionally, these methods are more applicable for this project due to the similarity of samples. Slight modifications were made to the O'Shay procedures due to time constraints because of the large number of samples processed. In brief, the procedures include destruction of basic minerals and leaching with strong acid (6M HCl), washing of samples with $CaCl_2$ solution, oxidation of samples with 30% H_2O_2, and titration of the resultant filtrate with NaOH to measure acid produced by minerals oxidized by H_2O_2. The NaOH used was standardized using potassium hydrogen phthalate.

All samples with handheld-XRF detectable sulfur levels were analyzed via ABA, as well as samples with no detectable amount of sulfur to provide full-scale coverage on possible sulfur content.

SEM was used to positively identify pyrite in the samples and to investigate the size and structure of the pyrite. It was also used to identify other trace minerals present in the samples. The instrument used was an FEI Quanta 600 FE-SEM in the Texas A&M University Microscopy and Imaging Center. Secondary electron images, backscatter electron images, and energy dispersive spectrometer data were gathered on 7 samples representing different mineral predominance.

FTIR spectral subtraction was performed using Spectrum™ software. A standard quartz spectrum obtained using similar parameters was used for subtraction. Differing intensities among spectra required subtraction to be performed in different ratios based on manual manipulation. Ratios of peak intensities before and after subtraction were compared to analyze the hidden peaks.

CHAPTER III

RESULTS AND DISCUSSION

A. Acid-Base Accounting

ABA results yield measurements in centimoles of H^+ produced per kilogram of sample (cmol/kg). This value represents the H^+ produced during H_2O_2 oxidation of minerals, presumably FeS_2. *Table 1* shows that the relative content of pyrite was often very small (usually <1% by mass) in these samples. However, these sediments still produced a large amount of acid drainage, resulting in groundwater with pHs of under 3. Acid mine drainage is a significant problem here due to trace quantities of pyrite. This finding is significant because XRD is often the primary investigative tool used for mineralogical research, but its detection limit is usually around 2% (Jeans, et al., 1997). This value is consistent with our data, as XRD was only able to effectively identify pyrite peaks in a few samples. This limitation is the main reason why FTIR was investigated as a tool for pyrite identification.

The calculation of cmol(H^+)/kg was performed using the formula developed in Sobek, et al. (1978). Via the oxidation reaction shown above results in 4 H^+ will be generated for each equivalent of FeS_2 oxidized by H_2O_2. The formula is as follows:

$$ABA\,(cmol(H+)/kg) = \frac{NaOH\,added(mL) \cdot Molarity\,NaOH(M) \cdot 100}{Mass\,soil(g)} \qquad (2)$$

Table 1. Complete list of samples and their ABA results showing percent composition of FeS_2 in the samples.

Sample:	Short ID:	$Mass_{dry}$ (g):	[NaOH]:	NaOH Added (mL):	H^+ Content (cmol/kg):	FeS_2 (% soil):
21-16_12.5-13.0	**H**	0.7262	0.01017	5.5	7.70	0.23%
25-16_4.8-5.3	**M**	0.77	0.01017	39.8	52.57	1.58%
25-16_7.0-7.5	**N**	0.8214	0.01017	19.7	24.39	0.73%
25-16_8.4-8.9	**O**	0.8464	0.01017	20.7	24.87	0.75%
25-16_14.4-14.9	**P**	0.8701	0.01017	16.8	19.64	0.59%
30-16_10.2-10.7	**Y**	0.754	0.01017	15.7	21.18	0.64%
23-16_5.0-5.5	**L1**	0.6711	0.00824	3.96	4.86	0.15%
23-16_6.8-7.3	**M1**	0.853	0.00824	51.51	49.76	1.49%
23-16_8.2-8.7	**N1**	0.7622	0.00824	37.93	41.01	1.23%
23-26_10.7-11.2	**O1**	0.779	0.00824	11.5	12.16	0.36%
23-16_12.5-13.0	**P1**	0.7231	0.00824	6.7	7.63	0.23%
23-16_12.5-13.0	**P1***	0.7154	0.00824	6.26	7.21	0.22%
18-16_8.2-8.7	**Q1**	0.7999	0.00824	4.19	4.32	0.13%
18-16_10.5-11.0	**R1**	0.7661	0.00824	2.79	3.00	0.09%
18-16_24.3-24.8	**S1**	0.7741	0.00824	5.91	6.29	0.19%
18-16_36.4-36.9	**T1**	0.808	0.00824	27.11	27.65	0.83%
18-16_36.4-36.9	**T1***	0.847	0.00824	35.09	34.14	1.02%
18-16_44.4-44.9	**U1**	0.8159	0.00824	5.64	5.70	0.17%
18-16_44.4-44.9	**U1***	0.7786	0.00824	4.1	4.34	0.13%
21-16_4.5-5.0	**AB1**	0.7322	0.00824	4.61	5.19	0.16%
19-16_2.5-3.0	**A2**	0.6076	0.01044	3.09	5.31	0.16%
19-16_6.1-6.6	**B2**	0.6288	0.01044	15.7	26.07	0.78%
19-16_13.0-13.5	**C2**	0.6788	0.01044	11.37	17.49	0.52%
19-16_14.2-14.7	**D2**	0.657	0.01044	2.97	4.72	0.14%
20-16_0.5-1.0	**E2**	0.6881	0.01044	5.08	7.71	0.23%
20-16_4.1-4.6	**F2**	0.6343	0.01044	4.39	7.23	0.22%
20-16_10.3-10.8	**G2**	0.7024	0.01044	3.45	5.13	0.15%
20-16_26.4-26.9	**H2**	0.7346	0.01044	3.89	5.53	0.17%
22-16_2.2-2.7	**J2**	0.6811	0.01044	5.36	8.22	0.25%
22-16_5.2-5.7	**K2**	0.6675	0.01044	2.5	3.91	0.12%
22-16_10.1-10.6	**L2**	0.7081	0.01044	20.11	29.65	0.89%

ABA results were compiled and compared to XRF data giving total sulfur content. These data were compared to determine the percent H^+ generated by pyrite, assuming all sulfur present in the sample is in the form FeS_2. This assumption should be relatively accurate, as leaching with $CaCl_2$ earlier in the procedure should have removed all soluble forms of sulfur. In the

majority of samples, the H^+ produced could not be accounted for solely by the FeS_2 content as calculated from XRF data. These results initially suggested that there must be interference in either ABA values or sulfur content determination.

The first hypothesis was that organic matter and organic sulfides were interfering with calculations. Sulfur in "low-sulfur" coals such as this lignite was derived primarily from sulfur in cysteine in prehistoric plants (Calkins, 1994); therefore, organic sulfur compounds are very likely to be found in these samples. The hypothesis of interfering organic sulfur compounds was rejected after further investigation. Organic sulfides are usually oxidized by H_2O_2 to sulfoxides or sulfones under laboratory conditions (Nyamunda, et al., 2013). Secondary sulfides are oxidized via a disproportionation of H_2O_2 to their sulfone derivatives, which is not an acid-forming reaction (Chu, 2004, and Brown, 1996). Alternatively, the oxidation of primary sulfides has potential to produce 1 equivalent of H^+ (Bach, et al., 1994). This could be a contributing factor to ABA results; however, the acid formed from primary organic sulfur is likely contribute a very small amount of the acid when compared to FeS_2. Samples with over 40g lignite per kilogram of sediment show unpredictable acid generation during ABA due to intermediate acidic products formed from incomplete oxidation (O'Shay, et al. 1990). This effect was seen on sample T1, which was rich in lignite as evidenced by its FTIR spectrum (*Figure 16* below).

Another hypothesis which we failed to reject was that the handheld XRF data was not accurate. This hypothesis is supported by the discrepancy between XRF sulfur content and ABA results (*Figure 4*). Another major limitation is that the detection limit of handheld XRF instruments for sulfur is quite high—resulting in the majority of samples in this study receiving a value of "not detectable" for sulfur content. Some of these samples had significant ABA values. Finally, representative samples were prepared in XRF capsules and re-measured with the

handheld device. The measured sulfur contents were around 3 times as high as those measured by in situ methods. This shows the limitation in application of handheld XRF devices for determination of sulfur content without laboratory preparation.

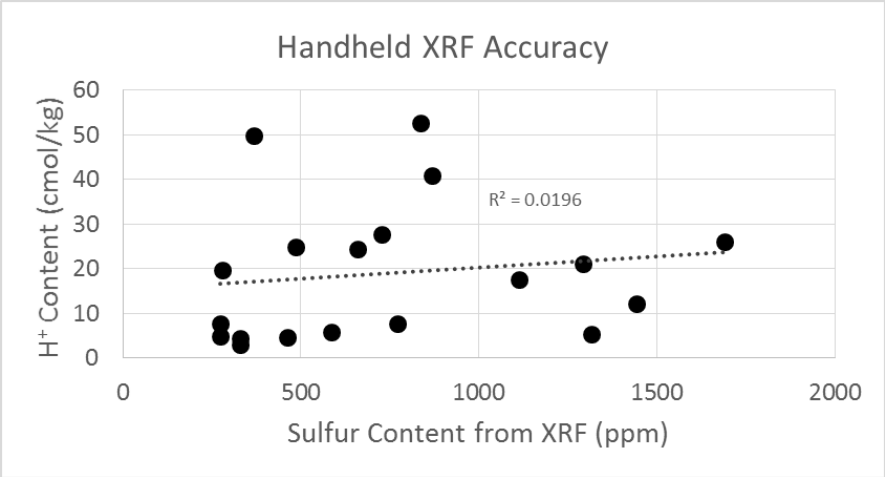

Figure 4. Graph showing poor relationship between XRF sulfur reading and ABA result.

Repetitions were performed for the samples "P1", "T1", and "U1". These repetitions were made to determine method reproducibility, and standard deviations were calculated. Unfortunately, due to time and reagent constraints, more repetitions were not run. P1, T1, and U1 represent medium, high, and low sulfur contents, respectively. The relative standard deviations for these samples were 4.05%, 14.86%, and 19.12%. Only two fractions were taken for each sample, which accounts for the high standard deviations seen in T1 and U1. Additionally, T1 is a sample very high in lignite, and the ABA value is therefore difficult to measure. These standard deviation values are likely responsible for some deviations from ideality in proposed trends. ABA results were used as a measure of pyrite content during subsequent SEM and FTIR methods.

It is worthwhile to point out the relationship between sediment depth and ABA value. Most of the high-ABA samples were found in depths from 5-15 feet, while the samples taken from the shallower and deeper regions showed a lower ABA value (*Figure 5*). This could be due to several factors. The first is that the rate of oxygen and water movement through the profile might result in intermediate depths not leaching well. Additionally, this could be due to a less permeable intermediate region which slows groundwater flow and could allow re-precipitation of secondary pyrite, leading to a build-up of AFM's in this depth interval. Remediation and revegetation efforts often only focus on the topsoil (~4 foot depth), and this could result in the clean-up of the topsoil with an abrupt jump in pyrite content below the remediation zone. Finally, it could simply be due to the method of overburden management by the mining company. Further research should be conducted on this spatial relationship between depth and ABA and how that will affect acid seepage and future remediation strategies.

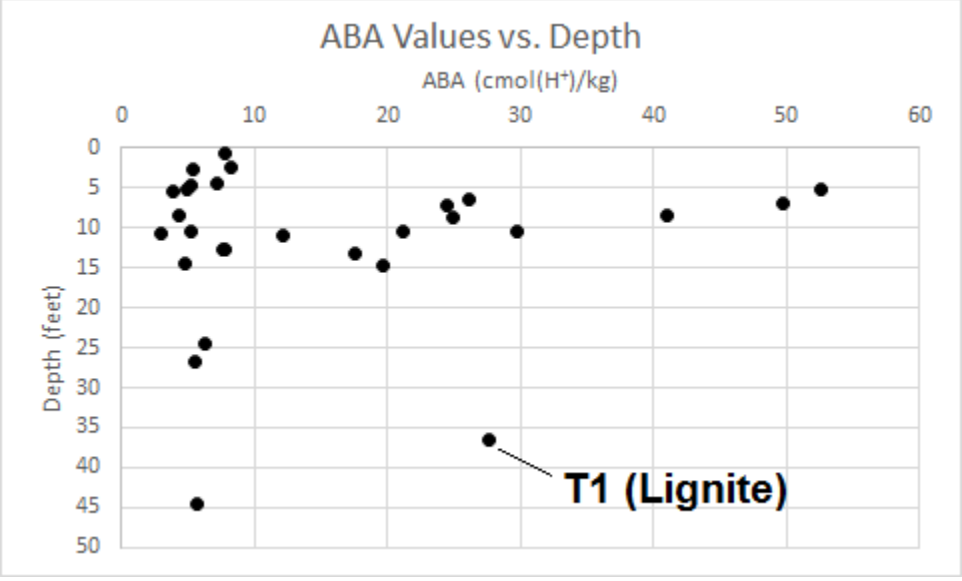

Figure 5. ABA values with sample depth. High ABA values are seen from 5-15 feet. The outlier near 36 feet is T1, which is high in lignite content and has a questionable ABA value.

B. Scanning Electron Microscopy

SEM was used to positively identify FeS_2. Until performing SEM, identification of FeS_2 had been speculative and estimated. SEM provided solid proof of FeS_2 in the samples as well as insight into the structure and fractionation of the FeS_2 (*Figures 6-9*). Secondary electron images were taken and used to observe the surface structure of the minerals.

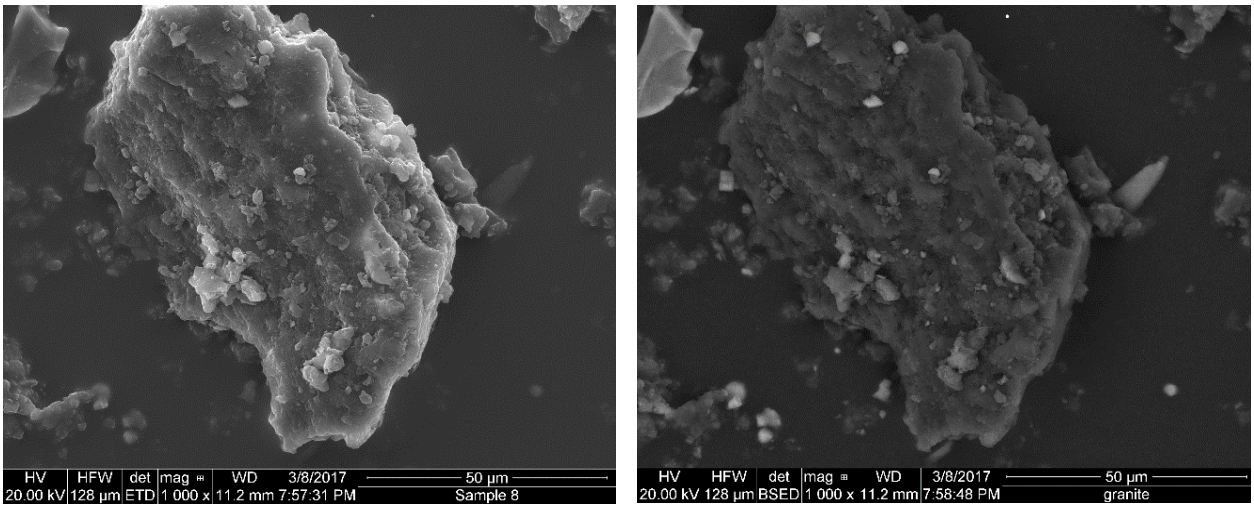

Figure 6 (above). Secondary (L) and backscatter (R) electron images of organic sediment from lignite (T1). The dark complexion in the images is due to low weight organics.

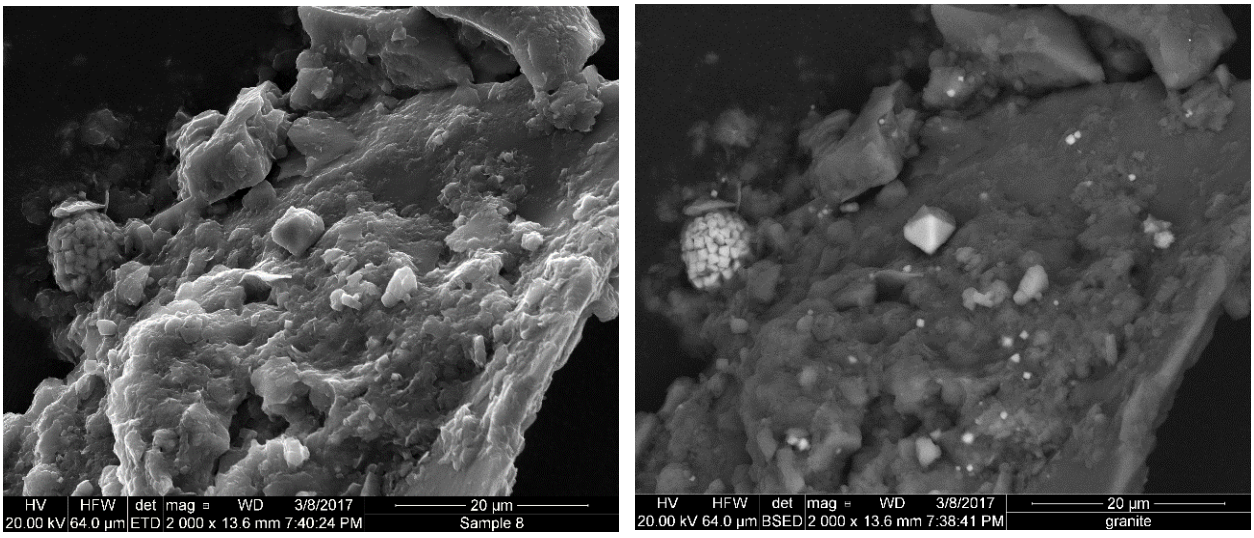

Figure 7 (above). Secondary (L) and backscatter (R) electron images of pyrite octahedral and framboidal structures on a quartz/aluminosilicate background (N1).

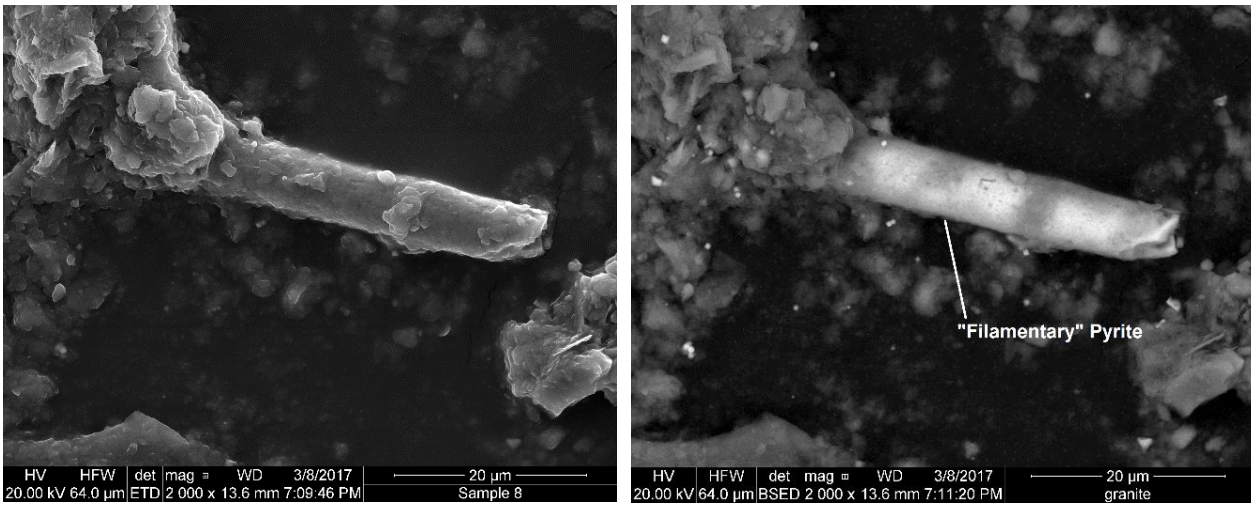

Figure 8 (above). Secondary (L) and backscatter (R) electron images of "filamentary" pyrite structure. This is an unusual and unexpected structure for pyrite (sample M1).

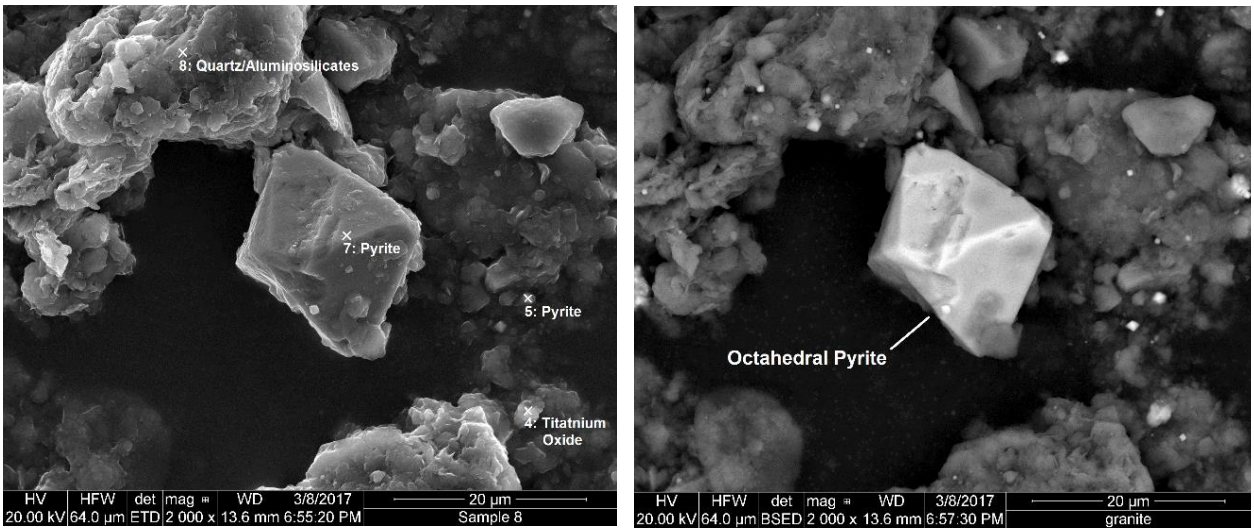

Figure 9 (above). Secondary electron image showing points of EDS sampling (L) and backscatter electron image showing octahedral pyrite crystal (R). Below in Figures 10-13 is seen the EDS results from the four measurement points. From sample M1.

Backscatter electron images were taken and used to find FeS_2 and target the minerals with the EDS to ensure proper identification (*Figures 10-13*).

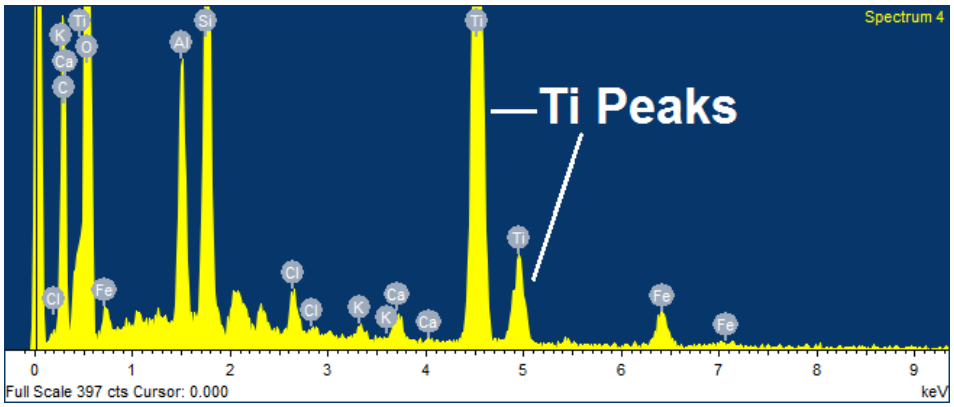

Figure 10. EDS spectrum showing predominance of titanium oxides at point 4 from Figure 9.

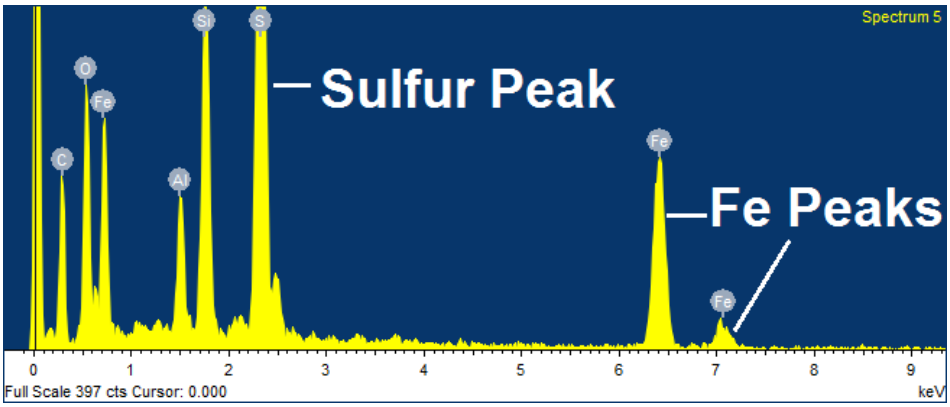

Figure 11. EDS spectrum showing predominance of pyrite at point 5 (R)—this is a clay sized octahedron.

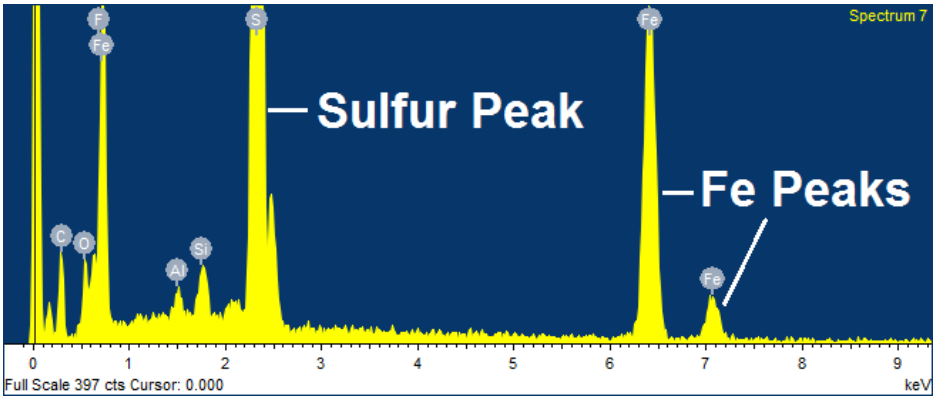

Figure 12. EDS spectrum showing pyrite result from the large octahedron at point 7.

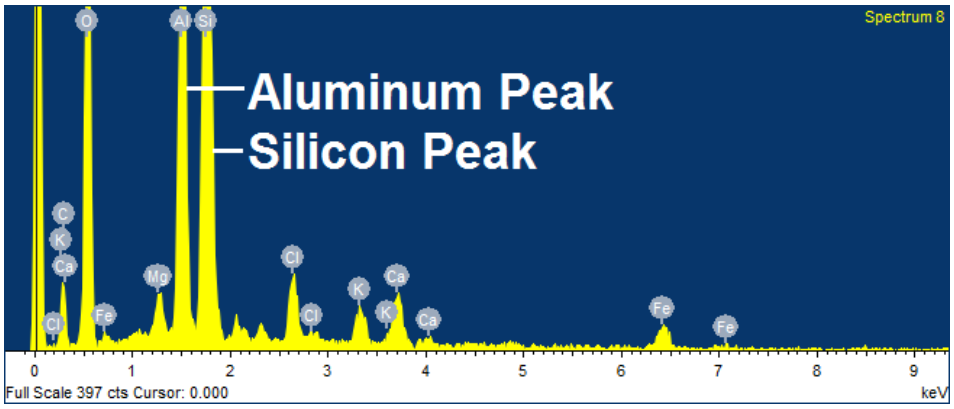

Figure 13. EDS spectrum showing predominance of quartz/aluminosilicate clays at point 8.

An interesting discovery was made during the SEM process. A relatively large "filamentary" pyrite structure was observed (*Figure 8*). Filamentary pyrite structures have been described before, but in that case they were associated with growing as inclusions into calcite crystals (Bonev, et al., 2005). Calcium was not detected in this sediment core section by the XRF, and the filament differs visually from that seen in the calcite deposit. FeS_2 is ideally cubic in structure, and it commonly weathers to the octahedral and framboidal structures seen above in *Figure 7*. This structure should be investigated for novel properties and to discover under what conditions it forms. SEM provided proof of FeS_2 presence in the sediments and also showed how small many of the crystals were—a property which will result in faster weathering and oxidation and could support the hypothesis of secondary pyrite precipitation in the medium-depth range.

C. Fourier-Transform Infrared Spectroscopy

Many of the FTIR patterns were very similar, depicting an abundance of either quartz (*Figure 14*), kaolinite (*Figure 15*), or a combination of the two minerals in the samples.

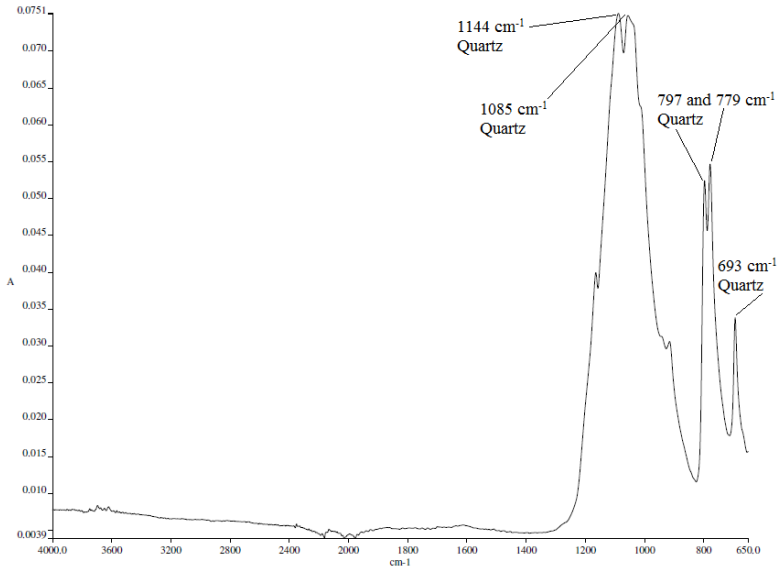

Figure 14. FTIR results from sample F determined to be nearly pure quartz.

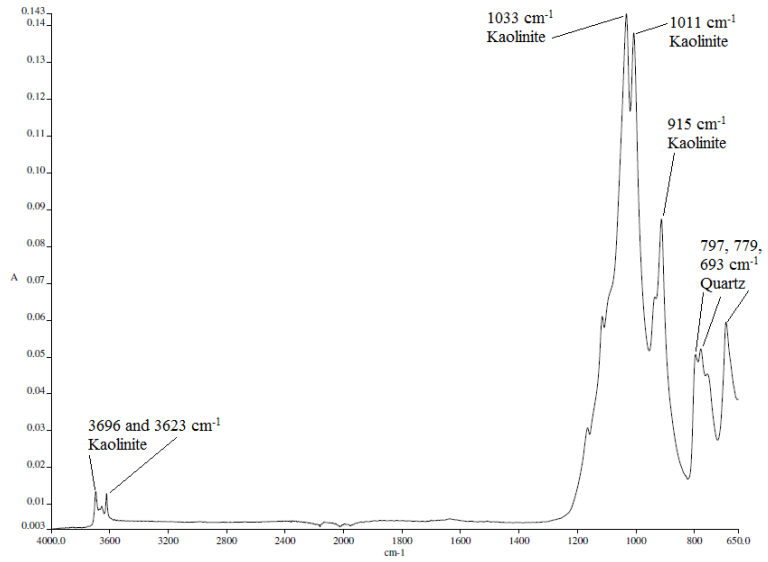

Figure 15. FTIR result from sample AC determined to be quartz with a substantial amount of kaolinite.

However, there is some variation among the samples. For instance, in *Figure 16* there is much reduced intensity from kaolinite or quartz, with numerous other peaks apparent due to organic materials. This sample is from a lignite-rich deposit. The broad peak seen around 1600 cm^{-1} is most likely due to amines, amides, asymmetrical alkenes, and aromatics. Also, the broad

peaks around 3200 and 1250 cm^{-1} are likely due to a mixture of alcohols and carboxylic acids. Furthermore, the spectrum in *Figure 17* contains several additional, well-defined peaks. These correlate to similar peaks seen in *Figure 16*, and are most likely due to a variety of organic molecules. The doublet at 2921 and 2848, and the broad peaks at 1598 and 1703 are often seen in these spectra, either prominent or barely visible.

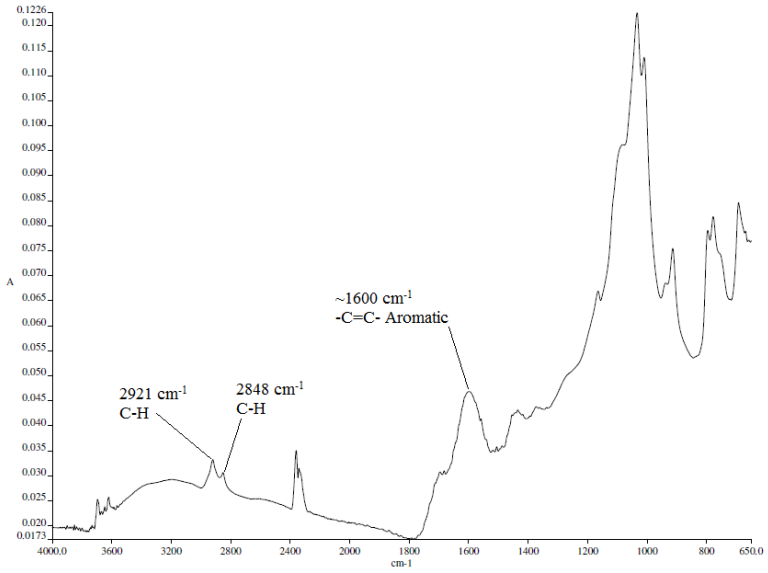

Figure 16. FTIR results from sample T1 *showing much variation in pattern due to organics (lignite) in addition to kaolinite and quartz..*

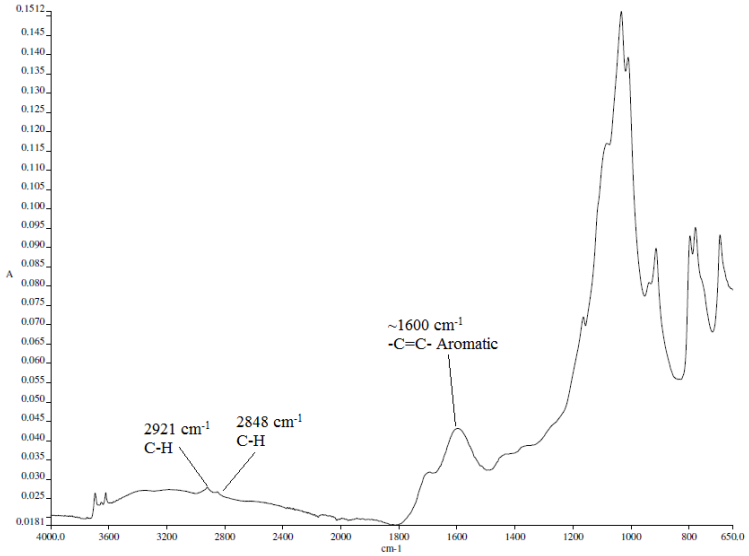

Figure 17. FTIR results from sample M showing a mixture of kaolinite, quartz, and organics.

As discussed above, spectral subtraction in FTIR is a useful technique in mineralogical applications (Puligilla, 2015, Maciejewska, 2015, and Predeanu, et al., 2016). Spectral subtraction was used with success in this project to investigate trace mineral peaks obscured by dominant mineral peaks. While kaolinite was common in the sediment samples at this site (as evidenced by the peaks at 3696 and 3623 cm^{-1}), quartz was present in large quantities in every sample. The primary peaks due to quartz are at 797, 779, and 693 cm^{-1}, while the peaks around 1033 and 1011 cm^{-1} are due to a combination of kaolinite and quartz.

The first subtraction trial involved subtracting samples with low ABA results, and hence, low pyrite content, from other samples with higher ABA results. Most notable, sample D1 was used. The results obtained were not repeatable or comprehensible, most likely due to matrix effects of subtracting out too many trace minerals. Due to the predominance of quartz and kaolinite in samples, efforts were then focused on subtracting out peaks due to these minerals. Standard pure kaolinite and quartz spectra were subtracted in varying proportions from the samples under study (*Figures 18* and *19*). Subtraction ratio was increased until characteristic peaks (3696 cm^{-1} for kaolinite and 693 cm^{-1} for quartz) were visually eliminated from the spectrum.

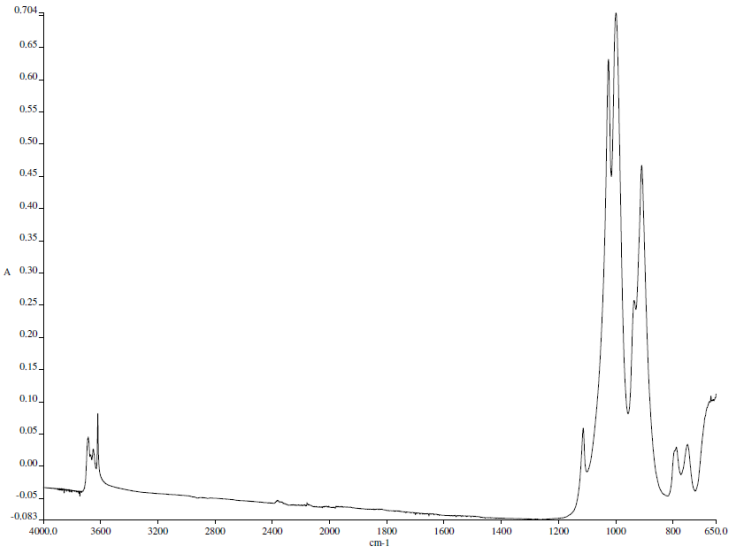

Figure 18. Standard spectrum of kaolinite used in attempts at spectral subtraction (above).

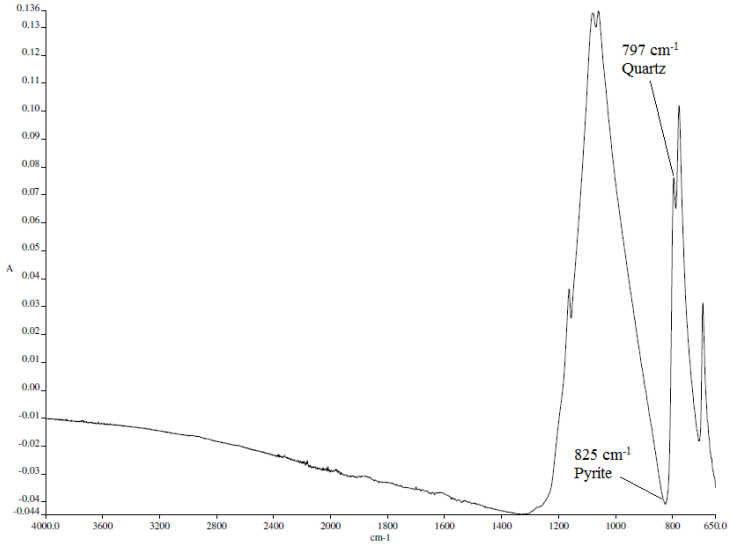

Figure 19. Standard spectrum of quartz used in subtraction. Highlighted are the specific wavelengths used in subtraction analysis (825 cm^{-1} for pyrite, 797 cm^{-1} for quartz).

After subtraction, several previously hidden peaks emerged. The most noticeable peaks were at 970 cm^{-1} and 825 cm^{-1}. Seen in *Figures 20, 21*, and *22* are spectra of samples L1, G2, and J2 before and after subtraction, showing the appearance of the 825 cm^{-1} peak in different magnitudes. These peaks were investigated in terms of their absorbance values compared to the

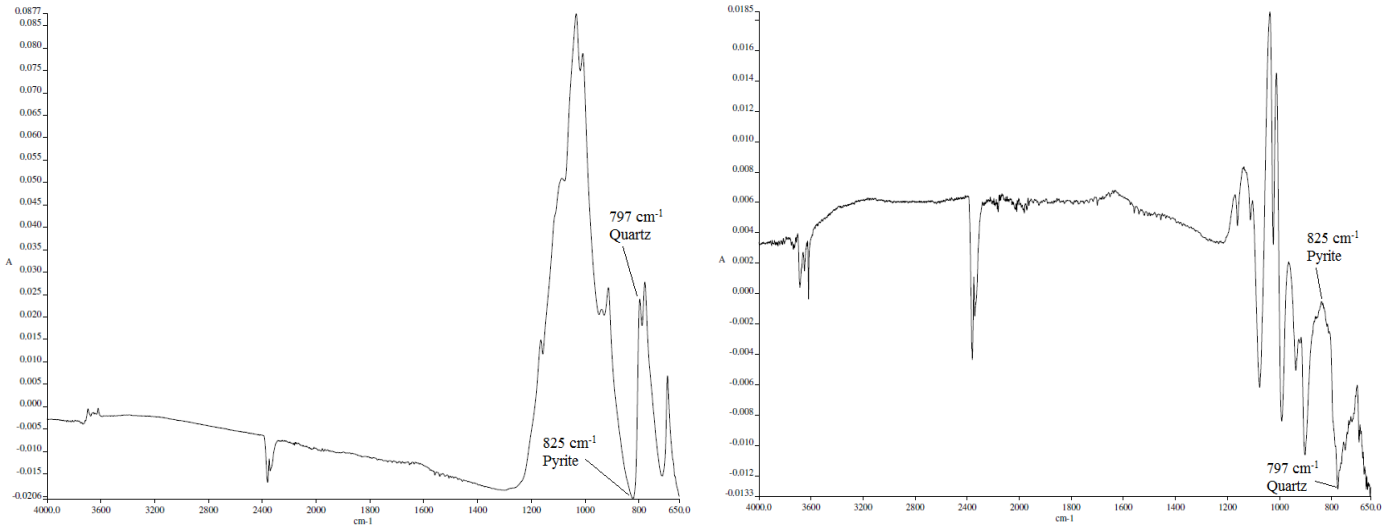

Figure 20. Original FTIR spectrum of sample L1 (left) and spectrum after subtraction of quartz spectrum (right) showing rise of 825 cm^{-1} peak.

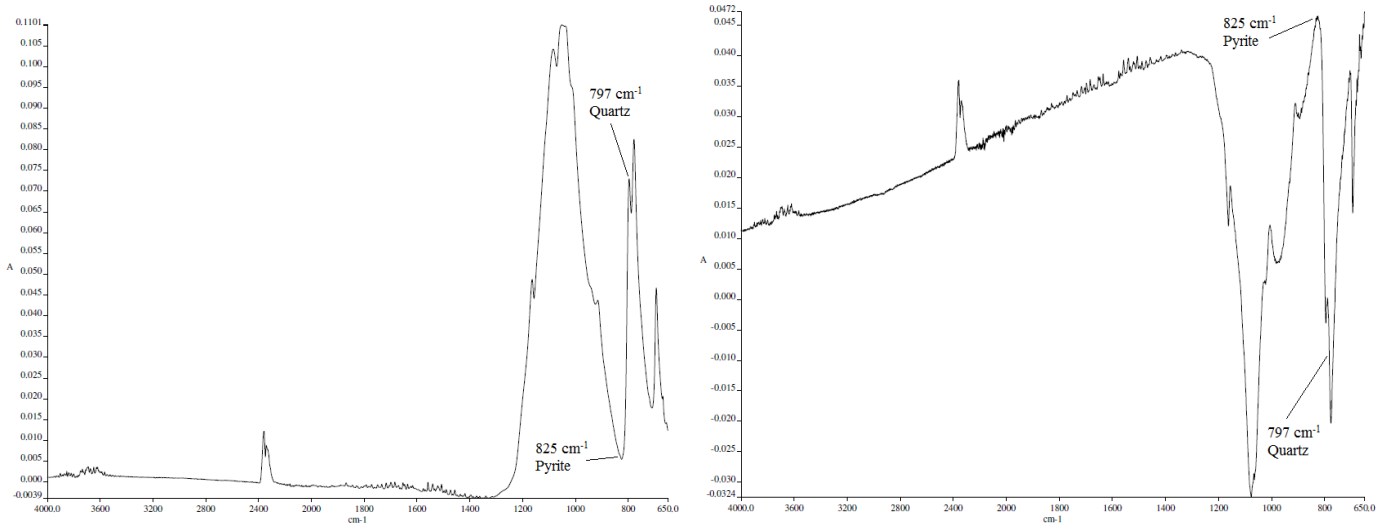

Figure 21. Original FTIR spectrum of sample G2 (left) and spectrum after subtraction of quartz spectrum (right) showing rise of 825 cm^{-1} peak.

absorbance values of the peaks having to do with kaolinite and quartz. The magnitude of absorbance of the 825 cm^{-1} peak was shown to be related to acid forming potential. Whenever a ratio of the change in absorbance of the 825 cm^{-1} after subtraction was compared to the change in absorbance of the 797 cm^{-1} quartz peak, a linear relationship to ABA value was seen (*Figure 23*

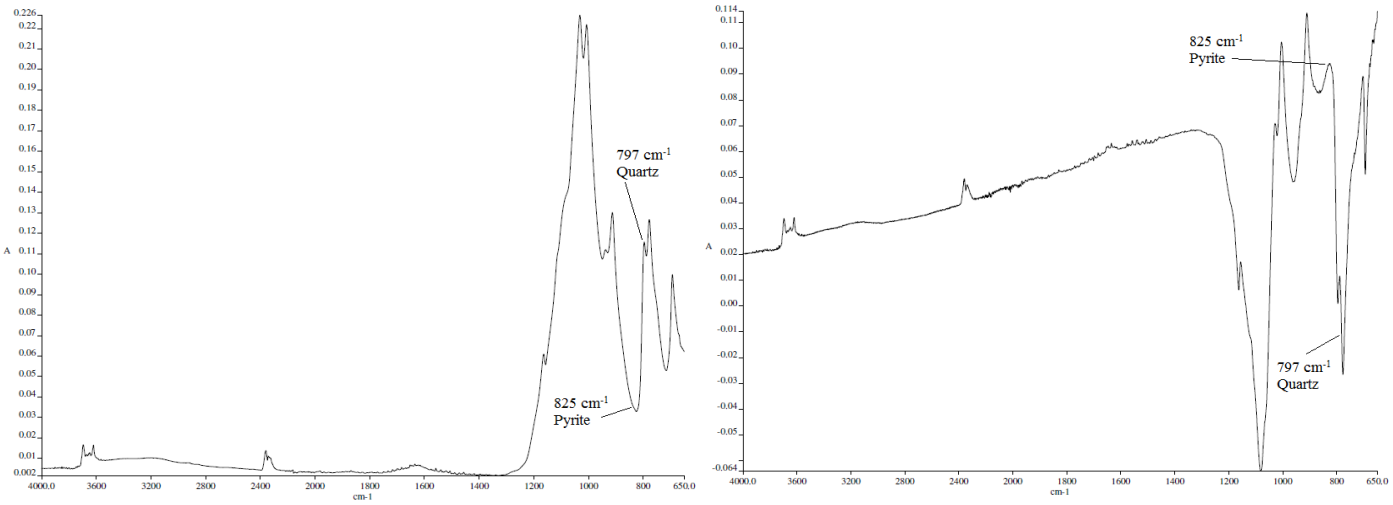

Figure 22. Original FTIR spectrum of sample J2 (left) and spectrum after subtraction of quartz spectrum (right) showing rise of 825 cm^{-1} peak.

and *Table 2*). The formula used for obtaining the –Δ825/Δ797 value is shown in the equation below. The negative value (-Δ825) is used simply to maintain a positive trend line slope.

$$\frac{-\Delta 825}{\Delta 797} = \frac{-(A825_o - A825_f)}{(A797_o - A797_f)} \quad (3)$$

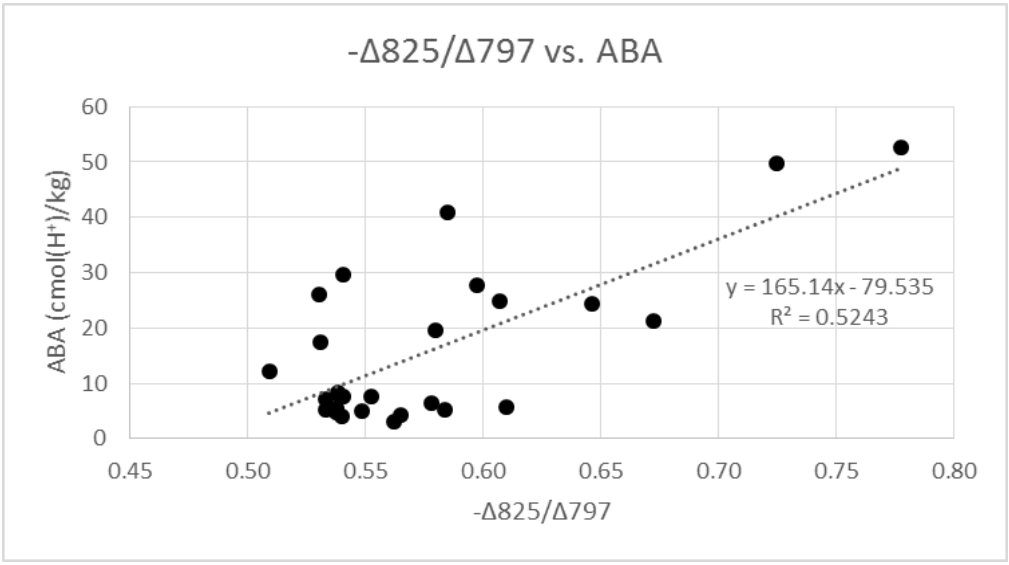

Figure 23. Linear relationship between the ratio of the change in 825 and 797 cm^{-1} peaks and ABA value.

Above is the formula used to calculate the x-axis value for *Figure 23* where $A825_o$ is the original absorbance at 825 cm^{-1}, $A825_f$ is the final absorbance at 825 cm^{-1} after subtraction, etc.

Table 2. Complete data set of absorbance values for the 825 cm^{-1} and 797 cm^{-1} peaks, ABA values, ratio values, and quartz ratio subtraction values (q).

Sample:	$A825_o$	$A825_f$	-Δ825	$A797_o$	$A797_f$	Δ797	q	ABA:	-Δ825/Δ797
H	0.050	0.112	0.062	0.120	0.005	0.115	1.5	**7.7**	0.5405
M	0.023	0.043	0.020	0.093	0.067	0.026	0.3	**52.57**	0.7778
N	0.022	0.043	0.021	0.070	0.037	0.033	0.4	**24.39**	0.6463
O	0.048	0.090	0.042	0.156	0.087	0.069	0.87	**24.87**	0.6072
P	0.030	0.062	0.032	0.113	0.057	0.056	0.7	**19.64**	0.5799
Y	0.036	0.066	0.030	0.091	0.046	0.045	0.528	**21.18**	0.6726
L1	-0.018	-0.001	0.018	0.024	-0.008	0.032	0.4	**4.86**	0.5488
M1	0.005	0.030	0.025	0.045	0.011	0.035	0.4	**49.76**	0.7246
N1	-0.001	0.026	0.027	0.047	0.001	0.045	0.55	**41.01**	0.5852
O1	-0.020	-0.010	0.010	0.008	-0.012	0.020	0.25	**12.16**	0.5095
P1	0.010	0.034	0.024	0.082	0.038	0.044	0.55	**7.63**	0.5525
Q1	-0.002	0.022	0.025	0.059	0.015	0.044	0.56	**4.32**	0.5651
R1	0.002	0.032	0.031	0.080	0.025	0.054	0.7	**3.00**	0.5626
S1	0.014	0.046	0.032	0.094	0.039	0.055	0.7	**6.29**	0.5782
T1	0.054	0.083	0.029	0.080	0.032	0.048	0.6	**27.65**	0.5975
U1	0.025	0.069	0.043	0.126	0.055	0.071	0.89	**5.70**	0.6099
AB1	-0.018	0.014	0.031	0.056	0.002	0.054	0.68	**5.19**	0.5840
A2	0.034	0.096	0.062	0.140	0.025	0.115	1.5	**5.31**	0.5334
B2	0.048	0.130	0.082	0.135	-0.019	0.154	2	**26.07**	0.5305
C2	0.041	0.123	0.082	0.136	-0.019	0.155	2	**17.49**	0.5310
D2	0.019	0.080	0.062	0.095	-0.020	0.115	1.5	**4.72**	0.5379
E2	0.044	0.106	0.062	0.096	-0.019	0.115	1.5	**7.71**	0.5397
F2	0.080	0.182	0.102	0.146	-0.045	0.191	2.5	**7.23**	0.5335
G2	0.006	0.047	0.041	0.073	-0.004	0.077	1	**5.13**	0.5367
H2	0.021	0.083	0.062	0.132	0.017	0.115	1.5	**5.53**	0.5382
J2	0.033	0.095	0.062	0.115	0.001	0.114	1.5	**8.22**	0.5385
K2	0.036	0.119	0.083	0.137	-0.016	0.153	2	**3.91**	0.5401
L2	0.045	0.120	0.074	0.114	-0.024	0.138	1.8	**29.65**	0.5407

The theoretical basis behind this discovery lies in the relative independence of the 825 cm^{-1} peak absorbance from the decrease in intensities seen at the peaks due to quartz. The low wavenumber tail from the quartz peak at 1011 cm^{-1} covers up any evidence of the 825 cm^{-1} peak in the original spectrum, and it is not until subtraction of the quartz peak that the size of the 825 cm^{-1} peak can be measured and related to ABA. The change in the 797 cm^{-1} quartz peak was used to offset any differences resulting from random variations in total absorbance from sample to sample and cause the 825 cm^{-1} peak absorbance to be a purely relative value of its intensity compared to the overall intensity of the spectrum. The 797 cm^{-1} peak was chosen because of its isolation from any other interfering peaks. Additionally, good results were shown when the change in the 825 cm^{-1} peak was compared to the change in the 3696 cm^{-1} peak whenever the standard kaolinite spectrum was subtracted. However, quartz was a better model standard in this project because of the abundance of quartz in every sample.

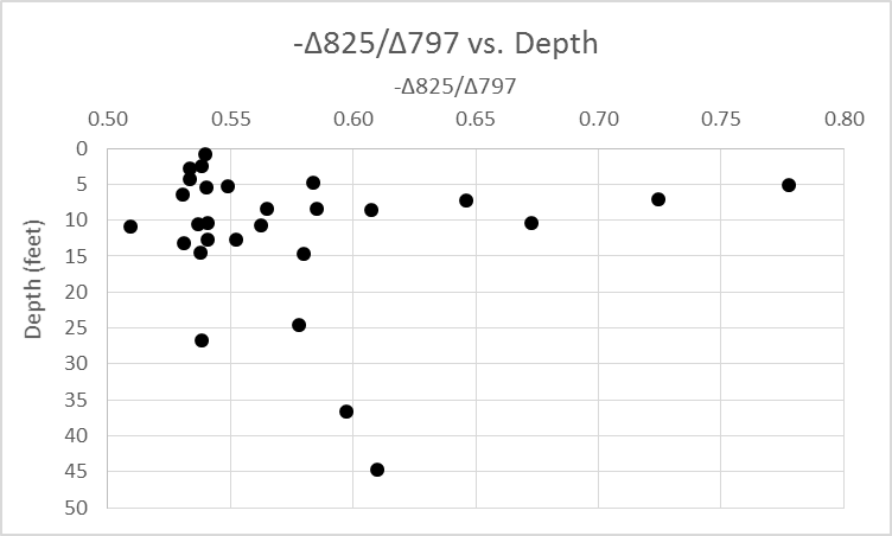

Figure 24. Recreation of Figure 5 with the –Δ825/Δ797 values replacing the ABA values. Graphs present a very similar trend—implying utility of using the –Δ825/Δ797 values.

FTIR spectra of pure pyrite have been shown to have a noticeable peak at 825 cm^{-1} (Marel, 1976). The presence of this peak in literature, the appearance of the peak after

subtraction of interfering minerals, and the peak's absorbance relation to the ABA value are strong evidence that this peak is due to FeS_2. Additionally, this is evidence that spectral subtraction of FTIR-ATR spectra can be used to detect FeS_2 in very low concentrations in sediments—even lower than the detection limit of XRD. Additionally, the $-\Delta 825/\Delta 797$ values can be compared to sample depth to regenerate a graph similar to that seen above (*Figure 5* and *Figure 24*).

CHAPTER IV

CONCLUSION

ABA results showed the connection between acid-forming potential and sample depth where samples from the 5-15 foot depth interval show the highest ABA result as compared to the samples above or below these. This finding should be investigated further and will help with current remediation efforts at the site.

As for methodology, handheld XRF measurements are incapable of providing accurate results of sulfur content to predict AFM. Additionally, trace quantities of FeS_2 in sediment samples (<1% often) can generate enough acid to cause a significant environmental problem. XRD is unable to accurately or positively identify FeS_2 in these trace quantities. SEM is often necessary for proper identification of FeS_2 in samples with low quantities of the mineral.

FTIR has been shown in this study to be capable of detecting trace FeS_2 quantities in sediments by detection of the 825 cm^{-1} peak which is in a relatively noise-free region. Subtraction of standard quartz spectra is necessary to elucidate this peak. Semi-quantitative data can be drawn from the relative decrease of this peak to predict acid formation—as the difference between the original and post-subtraction absorbance at 825 cm^{-1} increases in magnitude relative to the difference between the original and post-subtraction 797 cm^{-1} peak, the ABA result increases. This process could be used to predict acid formation before mining, to direct remediation efforts, or to create a strategy for treating overburden to prevent acid seepage. FTIR machines are relatively cheap and available, and are very fast compared to other mineralogical methods (SEM, XRD, or ABA) and thus could successfully be employed in the mining/remediation industry to provide relevant, quick data to assist in sustainable strategies.

Future work will attempt to develop relevant quartz (or other dominant mineral) spectra which are ideal for subtraction, and will work to create repeatable, mathematical methods of determining subtraction ratios to use so the process can be applied more generally with repeatability.

REFERENCES

Bach, R. D., et al. (1994). "Oxidation of Amines and Sulfides with Hydrogen Peroxide and Alkyl Hydrogen Peroxide. The Nature of the Oxygen-Transfer Step." *Journal of the American Chemical Society* **116**(12): 5379-5391.

Bonev, Ivan, et al. (2005). "Genesis of filamentary pyrite associated with calcite crystals." *European Journal of Mineralogy* **17**(6):905-913.

Brown, K. N. and J. H. Espenson (1996). "Stepwise Oxidation of Thiophene and Its Derivatives by Hydrogen Peroxide Catalyzed by Methyltrioxorhenium(VII)." Inorganic Chemistry **35**(25): 7211-7216.

Calkins, W.H. The chemical forms of sulfur in coal: A review. *Fuel* 1994, 73, 475–484.

Chu, J.-W. & B. L. Trout (2004). "On the Mechanisms of Oxidation of Organic Sulfides by H2O2 in Aqueous Solutions." Journal of the American Chemical Society **126**(3): 900-908.

Hossner, L.R., & Brandt, J.E. (1997). Acid/base account and minesoils: A review. United States: American Society for Surface Mining and Reclamation, Princeton, WV (United States). Accessed 9/13/2016 from http://www.osti.gov/scitech/biblio/613823.

Jeans, C., Moore, D. M. & Reynolds, R. C., Jr. 1997. X-Ray Diffraction and the Identification and Analysis of Clay Minerals, 2nd ed. xviii 378 pp. Oxford, New York: Oxford University Press. *Geological Magazine, 135*(6), 819-842.

Maciejewska, Aleksandra. Influence of Spectral Interferences on the Results of Quartz Determination by Infrared Spectrometry. Medycyna Pracy Volume 66, 04/2015: pp. 497–509. Department of Environmental Health Hazards. Łódź, Poland.

Marel, H.W. van der and Beutelspacher, H. (1976). *Atlas of Infrared Spectroscopy of Clay Minerals and their Admixtures*. Amsterdam: Elsevier Scientific Publishing Company.

McClure, J. R. 2012. Mineralogy and geochemistry of Pb, Zn, and Ag mine tailings originating

from carbonate-rich deposits. M.S. thesis. Texas A&M Univ., College Station.

Mittal, A. K. (2011). Abandoned Mines: Information on the Number of Hardrock Mines, Cost of Cleanup, and Value of Financial Assurances. U. S. G. A. Office.

Moses, C. O., et al. (1987). "Aqueous pyrite oxidation by dissolved oxygen and by ferric iron." Geochimica et Cosmochimica Acta **51**(6): 1561-1571.

Nyamunda, B.C., Chigondo, F., Moyo, M., Guyo, U., Shumba, M., Nharingo, T. (2013). Hydrogen Peroxide as an Oxidant for Organic Reactions. *Journal of Atoms and Molecules*, 3(1), 2013: pp. 23-44.

O'Shay, Tracey, Hossner, L.R., Dixon, J.B. (1990). A Modified Hydrogen Peroxide Oxidation Method for Determination of Potential Acidity in Pyritic Overburden. *Journal of Environmental Quality*, 19(4). Print.

Predeanu, G., et al. (2016). "Characterization of bottom ash of Pliocene lignite as ceramic composites raw material by petrographic, SEM/EDS and Raman microspectroscopical methods." International Journal of Coal Geology 168, Part 1: 131-145.

Puligilla, Sravanthi, Mondal, Paramita. *Co-existence of aluminosilicate and calcium silicate gel characterized through selective dissolution and FTIR spectral subtraction*, Cement and Concrete Research, Volume 70, April 2015, Pages 39-49.

Schaetzl, Randall and Anderson, Sharon. (2005). *Soils: Genesis and Geomorphology*. Cambridge: Cambridge University Press.

Sobek, Andrew A., Schuller, William A., Freeman, John R., Smith, Richard M. 1978. Field and Laboratory Methods Applicable to Overburdens and Minesoils. Environmental Protection Technology Series. Industrial Environmental Research Laboratory, Office of Research and Development. U.S. Environmental Protection Agency. Cincinnati, Ohio.

Thermo Nicolet Corporation, 2001. Introduction to Fourier Transform Infrared Spectroscopy. Thermo Nicolet. Retrieved 9/4/2016 from http://mmrc.caltech.edu/FTIR/FTIRintro.pdf

U.S. Environmental Protection Agency, 1994. Acid Mine Drainage Prediction. Office of Solid

Waste, Special Waste Branch. Retrieved 9/4/2016, from https://www.epa.gov/sites/production/files/2015-09/documents/amd.pdf

Xu, Z., Cornilsen, B. C., Popko, D. C., Wei, B., Pennington, W. D., & Wood, J. R. Quantitative Mineral Analysis by FTIR Spectroscopy. Retrieved September 04, 2016, from http://www.geo.mtu.edu/svl/pioneer/ftir/ftir_rpt.htm